Polarization-correction device with liquid crystals for quantum-key-distribution satellite systems

A. Jimenez-Girela,[1,*] D. Merino-Pérez,[1] A. Campos-Jara,[1] J. Socas Negrín,[2]
P. Garcia Parejo,[1] and A. Álvarez-Herrero[1]

[1] *Instituto Nacional de Técnica Aeroespacial (INTA), Carretera de Ajalvir km4, 28850 Madrid, Spain*
[2] *Instituto de Astrofísica de Canarias (IAC), 38205 La Laguna, Tenerife, Spain*

(Received 25 November 2024; revised 10 April 2025; accepted 21 May 2025; published 30 June 2025)

In this paper, we present a device, designed to be used in a space payload, capable of correcting any arbitrary polarization state. The device consists of a set of three liquid-crystal variable-retarder (LCVR) cells, in which by selecting the appropriate values of the voltage to be applied in each of them, it can correct the undesirable effects. In particular, the degradation effects of the polarization states, such as ellipticity and rotation with respect to the reference system, are compensated. Among many other potential applications, this device has been conceived to be used in quantum-key-distribution (QKD) intersatellite link or satellite-ground polarization-coding protocols as a polarization-correction device (PCD). To demonstrate that these effects are corrected, we have carried out an experiment in which we have tested how the BB84 protocol states are compensated after being strongly perturbed, achieving polarization extinction ratio (PER) values around 39 dB. Our solution offers the advantage of being small and mechanism free, being the ideal solution to be implemented in small satellites. These satellites are the core to be used in future constellations required for a global quantum communications network.

DOI: 10.1103/8plr-m6n8

I. INTRODUCTION

Liquid-crystal variable retarders (LCVRs) have been extensively used as light-polarization modulators for ground-based polarimetric applications. Our group is a pioneer in the development of these LCVRs for space applications, implementing this technology for European Space Agency (ESA) and NASA missions, such as the Solar Orbiter mission [1,2] or SUNRISE I-III [3–5]. In order to be used in these missions, we have qualified the LCVRs for space [6], obtaining, as relevant values, an ionizing-radiation tolerance of 100 krad, a vacuum environment of $< 10^{-6}$ mbar, and a survival temperature range of [$-40\,^{\circ}$C, $+90\,^{\circ}$C], and tested to withstand mechanical loads at launch. As a result of this development and their performance in space missions, our LCVRs have achieved a technological-readiness level (TRL) of 9, the TRL being scale used to measure the progress or maturity level of a technology [7].

The major potential that these LCVRs have in space is that they avoid the traditional rotatory polarizing optics and mechanisms, therefore reducing mass, volume, and power consumption. For an instrument on board a spacecraft, where resources are very limited and the risk of mechanical failure must be minimized, these are significant advantages. Besides, a device using electronic controls will always be faster than a mechanical one, which is essential in polarization-control operations. In addition, the device is proposed as ideal for use in small satellites where classical rotary mechanisms would be impossible to implement [8,9]. This opens up a huge potential for using constellations of small satellites, which are essential for a future global quantum communications network [10,11].

The potential applications in which liquid crystals can be used go beyond polarimetry, with uses for *in situ* magnetometers [12], quantum sensors in applications such as atom interferometry [13] and atomic clocks [14,15], and quantum communications [16,17]. Based on this extensive experience, a device that relies on this technology is proposed to be employed in quantum satellite communications. Specifically, in this paper we will be discussing how this device could be used in quantum-key-distribution (QKD) protocols based on polarization coding such as MICIUS [18,19]. In polarization-coding

*Contact author: ajimgir@inta.es

protocols, free-space and satellite quantum communications use photon polarization to carry the quantum states, in which the sender and receiver must share a common reference basis with respect to the polarization to obtain the secret key.

We realize that other polarization-control devices without moving components are available. One of the most important types are photoelastic modulators such as the one described in Ref. [20], developed by NASA. These devices are a competitor to those based on liquid crystals mainly due to their high modulation speeds [21]. The main problem with these devices is the high voltages that they require, in the order of hundred of volts, compared to the low voltages needed in liquid crystals which are below 14 V. This fact, coupled with a more complex calibration, makes them disadvantageous for inclusion in small satellites. The same disadvantages are present in other instruments based on Pockels and Kerr cells.

Unlike free-space ground-based quantum communications, where real-time polarization-base compensation is not necessary in most cases, in satellite quantum communications it is highly important, since the polarization base is dynamically changing due to the constant movement of the satellites in order to maintain the link [22]. Consequently, this will produce deflection and change the reference frame of the responding terminal, calling to this basis deviation [23]. In addition, both the optical elements of the system and atmospheric perturbations will inevitably deteriorate the polarization state of the quantum system, leading to an ellipticity in the polarization states that will decrease the polarization extinction ratio (PER).

Both effects, ellipticity and basis deviation, will lead to an increase in the quantum bit error rate (QBER) [24], making the channel more insecure and even inefficient for generating secure keys. This QBER is closely related to the PER and the basis deviation [22] as

$$\mathrm{QBER} = \frac{1}{\mathrm{PER}+1} + \frac{\mathrm{PER}-1}{\mathrm{PER}+1}\sin^2\theta, \tag{1}$$

where θ is the basis deviation measured in degrees. It is easy to see how the higher the PER is, the lower is the QBER. Therefore, a thorough study of how the PER of the system is reduced and how to avoid such a decrease becomes crucial.

The experimental results of the PER are usually expressed in decibels (dB). However, in order to use this value in Eq. (1), one should first convert the PER from a logarithmic to a linear scale. The relationship between the PER in decibels ($\mathrm{PER_{dB}}$) and the linear PER ($\mathrm{PER_{linear}}$) is given by

$$\mathrm{PER_{linear}} = 10^{\frac{\mathrm{PER_{dB}}}{10}}. \tag{2}$$

Although the use of liquid-crystal cells for polarization compensation has been performed in other studies [25], both the study with space-qualified cells and a study of the degree of polarization quantified by the PER is omitted in most works. To this end, in this paper, the performance of a polarization-correction device (PCD) based on space-qualified LCVRs is presented. In Sec. II, a theoretical explanation of the behavior of the PCD and how to calculate the retardance to achieve the optimal correction is provided. In Sec. III, the experimental setup will be explained. In Sec. IV, the experimental results of the PCD will be presented. Finally, in Sec. V, conclusions and possible applications of this device in the field of quantum communications in satellite systems will be presented.

II. THEORY

As mentioned in the previous section, the PCD is a device based on LCVRs capable of correcting both ellipticity and basis deviation in polarization states. The device is initially intended to be placed on Bob and correct these polarization states [26]. In addition, as a small module, it would also be ideal to increase the PER of the quantum states in small or portable optical ground stations. It is important to note that not all configurations of these LCVRs are capable of correcting any effect in a generic polarization state, but only specific configurations. A configuration that allows us to transform any input polarization state into any output polarization state [27], and is therefore able to correct all possible polarization errors, consists of a combination of three LCVR cells at the azimuthal positions of $\theta_1 = 0^\circ$, $\theta_2 = 45^\circ$, and $\theta_3 = 0^\circ$ (see Fig. 1) with respect to the horizontal plane and has been chosen because of the easier experimental setting.

To obtain the Mueller matrix of the system, the procedure described in Ref. [28] has been followed, obtaining for our case

$$M_{\mathrm{PCD}}(\delta_1,\delta_2,\delta_3) = \begin{pmatrix} 1 & 0 & 0 & 0 \\ 0 & \cos\delta_2 & \sin\delta_1\sin\delta_2 & -\cos\delta_1\sin\delta_2 \\ 0 & \sin\delta_2\sin\delta_3 & \cos\delta_1\cos\delta_3 - \cos\delta_2\sin\delta_1\sin\delta_3 & \cos\delta_3\sin\delta_1 + \cos\delta_1\cos\delta_2\sin\delta_3 \\ 0 & \sin\delta_2\cos\delta_3 & -\cos\delta_1\sin\delta_3 - \cos\delta_2\cos\delta_3\sin\delta_1 & \cos\delta_1\cos\delta_2\cos\delta_3 - \sin\delta_1\sin\delta_3 \end{pmatrix}, \tag{3}$$

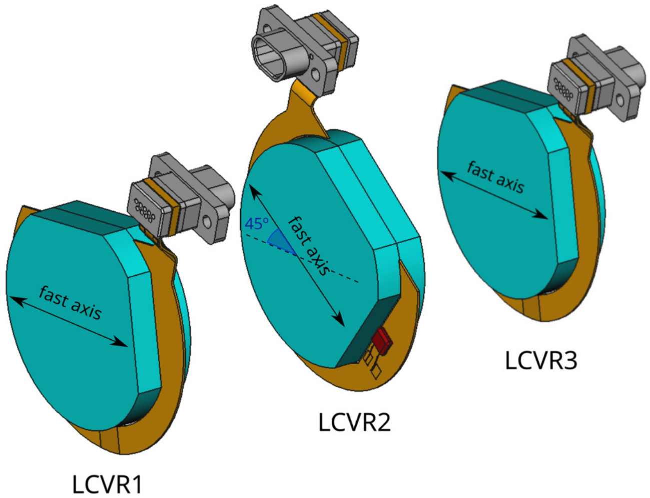

FIG. 1. The PCD architecture.

where δ_1, δ_2, and δ_3 are the retardances introduced by each LCVR.

Following the same formalism, it is simple to observe how this matrix corresponding to the PCD system must be the same as the inverse matrix representing the perturbation to be compensated, which is called $M_{\text{perturbed}}$:

$$M_{\text{PCD}}(\delta_1, \delta_2, \delta_3) = M^{-1}_{\text{perturbed}}, \tag{4}$$

where $M^{-1}_{\text{perturbed}}$ is the inverse matrix of the perturbation that has changed the polarization of the photon when it has passed through it. By solving this equation using numerical methods, we can obtain the set values (δ_1, δ_2, and δ_3) that correct the whole perturbation.

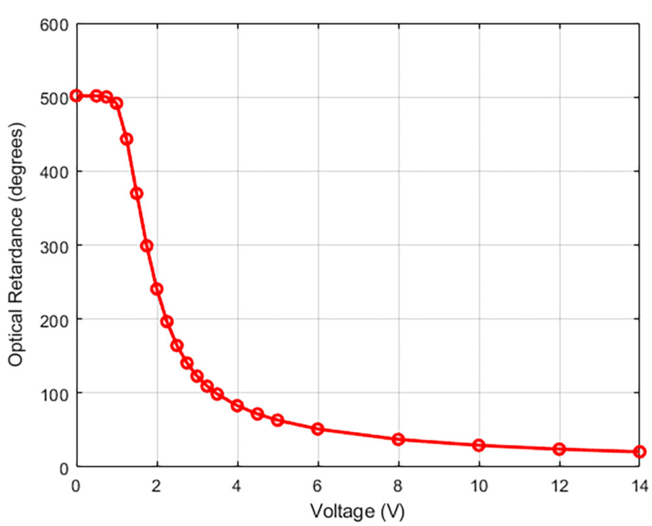

FIG. 2. The retardance-voltage curves of LCVR1 used in the experimental PCD. Similar curves have been obtained for LCVR2 and LCVR3.

Once the retardances to be included in each LCVR are known, it will be necessary to characterize them by obtaining their retardance-voltage relation in order to know which voltages need to be applied. The retardances of the LCVRs have been measured at 632.8-nm wavelength with a variable-angle spectroscopic ellipsometry (VASE) from J. A. Woollam. The characteristic curve can be seen in Fig. 2 (similar curves have been obtained for LCVR2 and LCVR3). The different voltages are shown on the X axis, while the retardances obtained by each voltage are shown on the Y axis.

III. EXPERIMENTAL SETUP

To validate the device, an experiment has been performed in which known initial polarization states have been perturbed and subsequently corrected. For this purpose, the experimental setup shown in Fig. 3, where the different optical elements are specified, has been used.

It is important to note that although, as mentioned above, real-time polarization-basis compensation is required, it is not necessary to do this for every polarization state emitted at the laser frequency. Considering that this device is initially conceived for a mission in which Bob is on a satellite in low Earth orbit, in the commissioning phase of the pass, the device is adjusted to the corresponding correction after an acquisition process of the received perturbed states of polarization. Then, the variations of the perturbation will be smooth—no very large changes will be necessary to correct the polarization—throughout the pass and of the order of tens of seconds, so the response times of our device, about tens of milliseconds [29], would not be a problem, as they would be 4 orders of magnitude lower. Therefore, the experimental results shown will take a static perturbation into account.

To generate the initial states (see Table I), a He-Ne laser at 632.8 nm has been used in combination with the polarization-eigenstates generator, the Meadowlark optics calibration set. This wavelength has been used because it was characterized in the experimental setup, but the device would work for any other wavelength—in particular, those used for quantum communications (808 nm, 850 nm, 1550 nm, etc.). This is because the wavelength change is not critical, as it would simply require optimization of the cells at that wavelength, i.e., that their antireflection coatings and thickness should have, at the very least, a 360° retardance curve.

Although the device can be used for any protocol that encodes information in polarization states, either prepare and measure or entanglement based, the initial states generated are of the BB84 protocol [30] with a PER between 45.8 and 46.8 dB. To perform the perturbation, a quarter-wave plate has been used, with its fast axis placed in an arbitrary position, being for this experiment 17° with respect to the horizontal axis chosen for the optical system.

TABLE I. The Stokes parameters measured for the initial input states.

Initial state	S_0	S_1	S_2	S_3
H	1.000	1.000	0.000	0.000
V	1.000	−1.000	0.000	0.000
D	1.000	0.000	1.000	0.000
A	1.000	0.000	−1.000	0.000

A polarization-state analyzer (PSA) from Meadowlark optics (model D3000 controller) has been used to measure the Stokes parameters and the basis deviation. It is important to note that the precision with which these Stokes parameters are measured is ± 0.001, so this is the maximum precision of the PSA. The PSA has been subjected to temperature control at 40 °C. This instrument would also be used to measure the PER. However, it is not possible to measure a value higher than 30 dB. To avoid this limiting our PER results, the Newport model 2936-C power meter has been used in conjunction with a high-contrast Glan-Thompson linear polarizer (shown in position 6 of Fig. 3 when the measure is performed), with contrast 1:100 000 (50 dB), to measure both the maximum and minimum intensity of each of the states and calculate the PER using

$$\mathrm{PER_{dB}} = 10\log_{10}\left(\frac{I_{\max}}{I_{\min}}\right). \tag{5}$$

Note that these intensities have been measured in the major ($I_{\max}$) and minor ($I_{\min}$) axes of the polarization ellipse, not using the standard horizontal-vertical (H-V) basis. This method has been used to compute the PER because it was measured with the power meter and not with the PSA that could have the H-V basis defined. Both methods of measuring the PER are equivalent, as shown in Ref. [24], in order to calculate the QBER.

The PCD, with its controller, is positioned to correct the perturbation generated by the quarter-wave plate. As mentioned previously, this PCD consists of three space-qualified LCVRs, each with a 30-mm clear aperture, response times of about tens of milliseconds, and an overall transmittance of approximately 89%. The three are housed in a mount (see Fig. 4) that provides active temperature control to keep them at 40 °C. This temperature has been selected because keeping the liquid crystal cells above room temperature enhances the internal dynamics of the liquid crystals and, therefore, provides the response times previously mentioned. We have also ensured, as shown in Fig. 2, that we have more than the required 360° of retardation.

The steps followed for the experiment are described as follows. First, the experimental matrix of the system that has perturbed the initial states has been obtained by measuring the output Stokes vectors using six known states, the four linear states of the BB84 protocol as well as the two circular ones:

$$M_{\text{perturbed}} = \begin{pmatrix} 1.000 & 0.000 & -0.001 & -0.013 \\ -0.003 & 0.656 & 0.532 & -0.513 \\ -0.001 & 0.455 & 0.271 & 0.855 \\ -0.006 & 0.577 & -0.812 & -0.070 \end{pmatrix}. \tag{6}$$

Following this, the Stokes and PER parameters of the perturbed states (see Table II) have been measured. The PCD has then been placed in position and the retardances

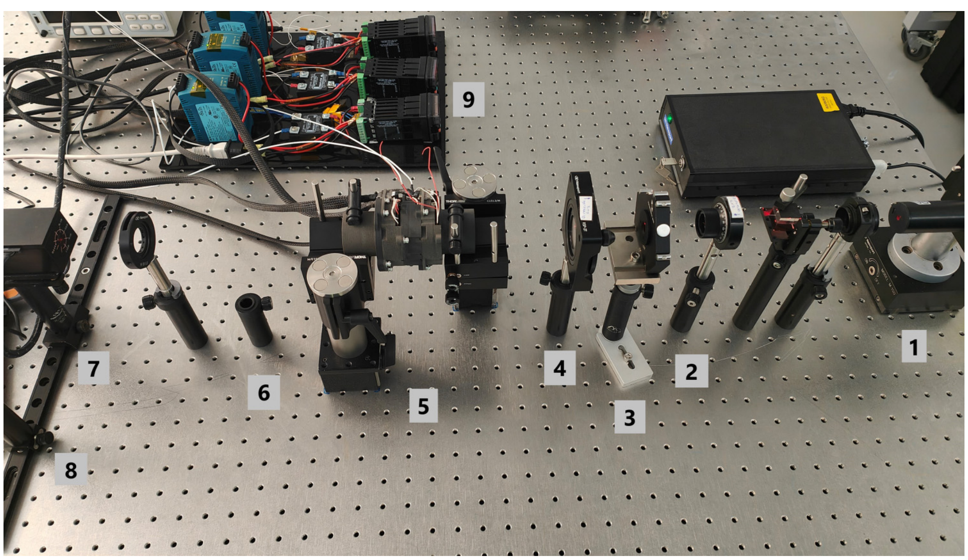

FIG. 3. The experimental setup: (1) He-Ne laser (632.8 nm), (2) quarter-wave plate, (3) polarized-state generator, (4) quarter-wave plate rotated by 17° with respect to the horizontal axis of the optical system, (5) PCD, (6) Glan-Thompson polarizer (7) PSA, (8) Newport power meter (model 2936-C), and (9) PCD controller.

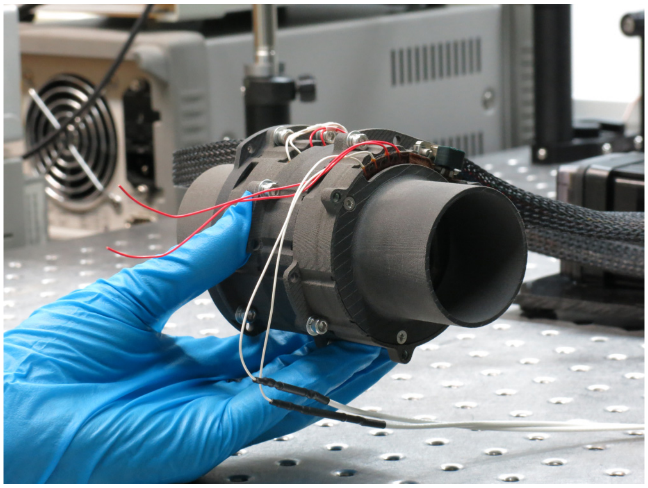

FIG. 4. The PCD mount that provides active temperature control.

of each cell have been determined using the process mentioned in Sec. II to obtain $M_{\text{perturbed}}^{-1}$. Once the calculated retardance for each LCVR has been set, the Stokes parameters and the PER of the corrected states have been measured. These values will be referred to as nominal values. Finally, following an improved version of the method described in Ref. [31], the new voltages of the LCVRs have been calculated to improve the results and fixed in each of them. This improvement comes from compensating deviations from an ideal system, the matrix shown in Eq. (3), and of the PCD itself, as well as the azimuth accuracy and nonideal effects of the LCVRs. Then, the measurements of the corrected states have been performed after applying the fine tuning to the nominal values, thus obtaining the final values of the Stokes parameters, the basis deviation, and the PER.

TABLE II. The Stokes parameters, PER, and basis deviation of the BB84 states at each experimental step.

	S_1	S_2	S_3	Basis deviation (degrees)	PER (dB)
Perturbed					
H	0.653	0.458	0.577	17.52	10.01
V	−0.665	−0.459	−0.582	17.22	9.86
D	0.536	0.272	−0.808	13.47	5.84
A	−0.522	−0.267	0.807	13.57	5.69
Corrected					
H	1.011	−0.017	0.003	0.49	39.11
V	−1.007	−0.003	0.008	0.11	39.07
D	−0.015	1.010	0.002	0.44	37.75
A	0.011	−0.983	0.003	0.32	39.17

IV. RESULTS

The numerical results are presented in Table II, where the experimental errors of these values are ±0.001 for the Stokes parameters and ±0.01 for the PER and basis deviation. The values of the Stokes parameters are normalized to S_0. We have chosen to present the results of perturbations that provided sufficient degradation in the PER. To illustrate these results, the values are represented in Fig. 5.

Looking at Table II, it is straightforward to see how the quarter-wave plate used to perturb the initial states reduces the PER by a factor of 7.9 in the worst cases (diagonal-antidiagonal, D-A) and by a factor of 4.6 in the best cases (H-V). After the correction introduced by the PCD and the application of fine tuning, PER values of more than

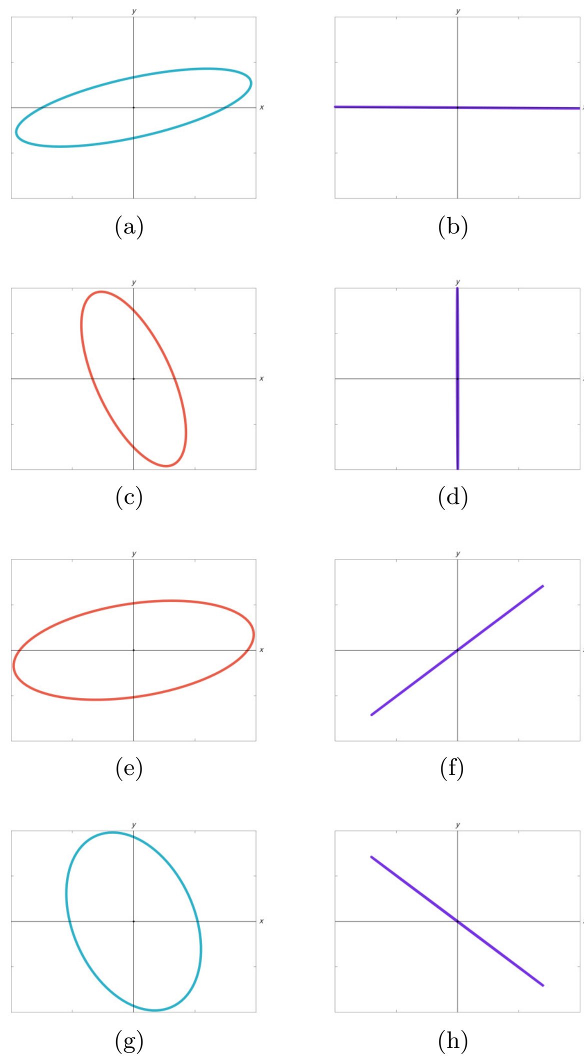

FIG. 5. The polarization ellipses of the BB84 states: (a),(c),(e),(g) representations of the perturbed states (H, V, D, and A, respectively); (b),(d),(f),(h) representations of the corrected states. The red color represents left-elliptical polarization, blue right-elliptical polarization, and purple linear polarization.

39 dB are achieved. It is important to note that although our test is performed in a simple way, we are introducing a strong perturbation. This strong perturbation, which is not expected in a real system, includes the representative contributions to the possible perturbations caused by a complete optical system.

It is important to remember that, as detailed in the previous section, both the Stokes-parameter values and the basis deviation have been obtained using the PSA, while the PER values have been obtained by measuring the intensities using the power meter.

Likewise, looking at the basis deviation, it can be seen how the perturbing system deviates the states up to a maximum of 17.5°, being subsequently completely corrected except for a marginal rotation by a maximum of 0.5° for the H state.

With these values of the PER and the basis deviation achieved in the corrected states, the QBER introduced by polarization is, using Eq. (1), only 0.02%. Therefore, the security bound of the BB84 protocol can be fulfilled [32]. These results show that since the polarization is almost completely corrected, it will not affect the QBER. Therefore, a wide margin is still available for other QBER contributions.

V. CONCLUSIONS

In conclusion, we have proposed a space-validated device based on liquid crystals that can be used in applications that require polarization control and correction. In particular, we have evaluated this device experimentally for use as a polarization corrector in space QKD systems based on polarization-coding protocols such as BB84 or BBM92. Furthermore, considering that the contribution to the QBER generated by the polarization error after correcting it using the PCD is less than 0.02%, it is concluded that the contribution to the QBER at a practical level is negligible, thus suggesting that the device should be ideal for use in these protocols.

As future research, the implementation of a closed-loop optimization algorithm focused on the search for voltages for the correction and tracking of polarization states in flight is proposed.

DATA AVAILABILITY

The data that support the findings of this paper are openly available [33]; embargo periods may apply.

[1] D. Müller *et al.*, The Solar Orbiter mission—science overview, Astron. Astrophys. **642**, A1 (2020).

[2] Ester Antonucci *et al.*, Metis: The Solar Orbiter visible light and ultraviolet coronal imager, Astron. Astrophys. **642**, A10 (2020).

[3] V. Martínez Pillet *et al.*, The Imaging Magnetograph eXperiment (IMaX) for the *Sunrise* balloon-borne solar observatory, Sol. Phys. **268**, 57 (2010).

[4] S. K. Solanki *et al.*, The polarimetric and helioseismic imager on Solar Orbiter, Astron. Astrophys. **642**, A11 (2020).

[5] A. Á. Herrero, A. Fernández-Medina, M. Cebollero, D. Garranzo-García, A. Núñez, A. Gonzalo, A. Sánchez, J. Villanueva, P. G. Parejo, A. Campos-Jara *et al.*, TuMag for SUNRISE III mission: Development of the optical unit of an imaging spectropolarimeter, in *Ground-Based and Airborne Instrumentation for Astronomy IX* (SPIE Astronomical Telescopes + Instrumentation, Montréal, Québec, Canada, 2022), Vol. 12184, p. 88.

[6] A. Alvarez-Herrero, N. Uribe-Patarroyo, P. G. Parejo, J. Vargas, R. L. Heredero, R. Restrepo, V. Martínez-Pillet, J. C. del Toro Iniesta, A. López, S. Finesch *et al.*, in *Polarization Science and Remote Sensing V*, Vol. 8160, edited by J. A. Shaw and J. S. Tyo, International Society for Optics and Photonics (SPIE, 2011), p. 81600Y.

[7] NASA, Technology readiness level definitions (2013), https://www.nasa.gov/pdf/458490main_TRL_Definitions.pdf, accessed January 29, 2025.

[8] E. Kerstel, A. Gardelein, M. Barthelemy, T. C. Team, M. Fink, S. K. Joshi, and R. Ursin, Nanobob: A CubeSat mission concept for quantum communication experiments in an uplink configuration, EPJ Quantum Technol. **5**, 6 (2018).

[9] S. P. Neumann, S. K. Joshi, M. Fink, T. Scheidl, R. Blach, C. Scharlemann, S. Abouagaga, D. Bambery, E. Kerstel, M. Barthelemy *et al.*, Q3Sat: Quantum communication uplink to a 3U CubeSat: Feasibility & design, EPJ Quantum Technol. **5**, 24 (2018).

[10] L. Mazzarella, C. Lowe, D. Lowndes, S. K. Joshi, S. Greenland, D. McNeil, C. Mercury, M. Macdonald, J. Rarity, and D. K. L. Oi, QUARC: Quantum research CubeSat—a constellation for quantum communication, Cryptography **4**, 7 (2020).

[11] D. K. Oi, A. Ling, G. Vallone, P. Villoresi, S. Greenland, E. Kerr, M. Macdonald, H. Weinfurter, H. Kuiper, E. Charbon *et al.*, CubeSat quantum communications mission, EPJ Quantum Technol. **4**, 6 (2017).

[12] J. Rutkowski, W. Fourcault, F. Bertrand, U. Rossini, S. Gétin, S. Le Calvez, T. Jager, E. Herth, C. Gorecki, M. L. Prado *et al.*, Towards a miniature atomic scalar magnetometer using a liquid crystal polarization rotator, Sens. Actuators A: Phys. **216**, 386 (2014).

[13] J. Fang, J. Hu, X. Chen, H. Zhu, L. Zhou, J. Zhong, J. Wang, and M. Zhan, Realization of a compact one-seed laser system for atom interferometer-based gravimeters, Opt. Express **26**, 1586 (2018).

[14] Y. Yano and S. Goka, Pulse excitation method of coherent-population-trapping suitable for chip-scale atomic clock, Jpn. J. Appl. Phys. **51**, 122401 (2012).

[15] P. Yun, F. Tricot, C. E. Calosso, S. Micalizio, B. François, R. Boudot, S. Guérandel, and E. de Clercq, High-performance coherent population trapping clock with polarization modulation, Phys. Rev. Appl. **7**, 014018 (2017).

[16] Z. Tang, R. Chandrasekara, Y. C. Tan, C. Cheng, L. Sha, G. C. Hiang, D. K. L. Oi, and A. Ling, Generation and analysis of correlated pairs of photons aboard a nanosatellite, Phys. Rev. Appl. **5**, 054022 (2016).

[17] J. T. Barreiro, T.-C. Wei, and P. G. Kwiat, Remote preparation of single-photon "hybrid" entangled and vector-polarization states, Phys. Rev. Lett. **105**, 030407 (2010).

[18] S.-K. Liao, W.-Q. Cai, W.-Y. Liu, L. Zhang, Y. Li, J.-G. Ren, J. Yin, Q. Shen, Y. Cao, Z.-P. Li *et al.*, Satellite-to-ground quantum key distribution, Nature **549**, 43 (2017).

[19] S.-K. Liao, W.-Q. Cai, J. Handsteiner, B. Liu, J. Yin, L. Zhang, D. Rauch, M. Fink, J.-G. Ren, and W.-Y. a. e. a. Liu, Satellite-relayed intercontinental quantum network, Phys. Rev. Lett. **120**, 030501 (2018).

[20] G. van Harten, D. J. Diner, B. J. S. Daugherty, B. E. Rheingans, M. A. Bull, F. C. Seidel, R. A. Chipman, B. Cairns, A. P. Wasilewski, and K. D. Knobelspiesse, Calibration and validation of airborne multiangle spectropolarimetric imager (AirMSPI) polarization measurements, Appl. Opt. **57**, 4499 (2018).

[21] F. A. Iglesias and A. J. Feller, Instrumentation for solar spectropolarimetry: State of the art and prospects, Opt. Eng. **58**, 082417 (2019).

[22] J. Wu, L. Zhang, J. Jia, T. Wang, R. Shu, Z. He, and J. Wang, Polarization-maintaining design for satellite-based quantum communication terminals, Opt. Express **28**, 10746 (2020).

[23] M. Zhang, L. Zhang, J. Wu, S. Yang, X. Wan, Z. He, J. Jia, D. S. Citrin, and J. Wang, Detection and compensation of basis deviation in satellite-to-ground quantum communications, Opt. Express **22**, 9871 (2014).

[24] J. Wu, Z. He, L. Zhang, L. Yuan, T. Wang, J. Jia, R. Shu, and J. Wang, Polarization study about a telescope-based transmitter for quantum communication, Appl. Opt. **56**, 8501 (2017).

[25] Y. Shi, H. S. Poh, A. Ling, and C. Kurtsiefer, Fibre polarisation state compensation in entanglement-based quantum key distribution, Opt. Express **29**, 37075 (2021).

[26] A. Jimenez-Girela, P. Arteaga-Díaz, D. Merino-Pérez, P. Garcia-Parejo, S. Rodríguez-Bustabad, T. Belenguer-Dávila, V. Fernández-Mármol, and A. Álvarez-Herrero, Inflight demonstrator of quantum key distribution between CubeSats of Q-ANSER program, in *Photonics for Quantum 2023*, edited by D. F. Figer and M. Reimer, International Society for Optics and Photonics (SPIE, Rochester, New York, United States, 2023), Vol. 12633, p. 126330C.

[27] Z. Zhuang, S.-W. Suh, and J. S. Patel, Polarization controller using nematic liquid crystals, Opt. Lett. **24**, 694 (1999).

[28] D. H. Goldstein, *Polarized Light, Third Edition* (CRC Press, 2011).

[29] A. Campos de España Jara, P. Parejo, and A. Alvarez-Herrero, Optimization of the response time measuring method for liquid crystal variable retarders, J. Vac. Sci. Technol. B **37**, 062930 (2019).

[30] C. H. Bennett and G. Brassard, Quantum cryptography: Public key distribution and coin tossing, Theor. Comput. Sci. **560**, 7 (2014).

[31] A. Álvarez Herrero, P. G. Parejo, and M. Silva-López, Fine tuning method for optimization of liquid crystal based polarimeters, Opt. Express **26**, 12038 (2018).

[32] P. W. Shor and J. Preskill, Simple proof of security of the BB84 quantum key distribution protocol, Phys. Rev. Lett. **85**, 441 (2000).

[33] The DOI to acces de publish data is https://doi.org/10.5281/zenodo.15348919.